State-Space Analysis of the Quantum-Well Injection Transit Time Diode

David R. Conn, *Member, IEEE*, and Paul D. Bauman

Abstract—**A state-space linear model of the quantum-well injection transit time (QWITT) diode is developed in this paper. The resulting system of equations are suitable for time- and frequency-domain analysis of the QWITT diode with its external circuit, and since the eigenvalues (complex resonant frequencies) are an integral part of the formulation, the method is extremely useful for the design of oscillator circuits and for the study of stability problems that are associated with supplying bias to the diode. The model includes the effects of velocity overshoot and carrier diffusivity, as well as the physical geometry of the devices being studied. It is tested by comparing the predicted small-signal impedance with other well-known models for similar devices. Using state-space analysis, it is predicted that long diodes with a positive injection conductance will not have an input impedance with a negative real part at any frequency.**

I. Introduction

THE quantum-well injection transit time (QWITT) diode shows considerable promise for millimeter-wave applications [1]–[6] and for integrated antenna systems that require mixers, oscillators, and control elements. In the QWITT diode structure, a double-barrier quantum well is used as an emitter of electrons that pass through a depleted region which supports drift, diffusion, and displacement currents. The QWITT diode structure that we have studied from both a theoretical and an experimental viewpoint is shown in Fig. 1 along with the measured $I-V$ characteristics of a typical device.

Accurate large- and small-signal device models are required for the QWITT diode for several reasons. Most importantly, the integration of these devices with GaAs circuits requires a complete device/circuit simulation for the prediction of the overall system response. Also, low-frequency oscillations caused by bias lines and diode mounting structures can only be understood and thus controlled through the use of accurate models that include transit time effects, drift and diffusion currents, and realistic assumptions about the diode geometry and parasitic resistances.

Botula *et al.* [7] have extended the small-signal modeling of Kesan *et al.* [8] for the QWITT diode, which followed the original analysis of Read [9] and of Gilden and Hines [10] for IMPact Avalanche Transit Time (IMPATT) diodes. Recently, Kidner *et al.* [11] have addressed the problem of power and low-frequency stability in the QWITT diode, where they use a nondistributed lumped element model for both the diode and the external circuit. They conclude that stable resonant tunneling diode operation is difficult to obtain and that there is a significant trade-off between power generation and stability.

This paper presents a complete state-space model of the QWITT diode that is suitable for time- and frequency-domain analysis of the diode with its external circuit. Since the eigenvalues (resonant frequencies) are an integral part of the analysis, the problem of device/circuit stability is readily addressed using this technique. The state-space technique is also useful for the design of oscillators where the damping factor as well as the oscillating frequency is required. Section II of this paper gives a short description of state-space techniques and shows how the state variables (electric field in the injection and drift regions) can be used in either the frequency or the time domain. Section III describes the method of dealing with carrier velocity and diffusivity as a function of distance in the drift region. We use the same assumptions employed by Botula *et al.* [7] in order to confirm the state-space method of analysis with respect to an analytic solution. This constraint is easily removed for the study of other devices and materials or if greater modeling accuracy is required for the existing structure. The state-space model of the diode is developed in Section IV and is compared with previous analysis techniques in Section V. New results obtained using the state-space method of analysis are presented in Section VI. Here it is demonstrated that long devices with positive injection conductance do not produce a negative real part of the input impedance, as previously reported [8]. Long devices become inactive as a consequence of nonconstant velocity and diffusion in the drift region, and the obtained results are in agreement with those reported by Song and Pan [12].

II. The State-Space Analysis Technique

The state-space [13] technique is a systematic approach for analyzing a linear time-invariant differential system that can be described by a state vector $\boldsymbol{x}$ of dimension N. For this particular problem, the state vector $\boldsymbol{x}$ represents

Manuscript received October 16, 1990; revised March 5, 1991. This work was supported by Bell-Northern Research and by the Telecommunications Research Institute of Ontario.

The authors are with the Communications Research Laboratory, McMaster University, Hamilton, Ontario, Canada L8S 4K1.

IEEE Log Number 9100850.

0018-9480/91/0800-1403$01.00 ©1991 IEEE

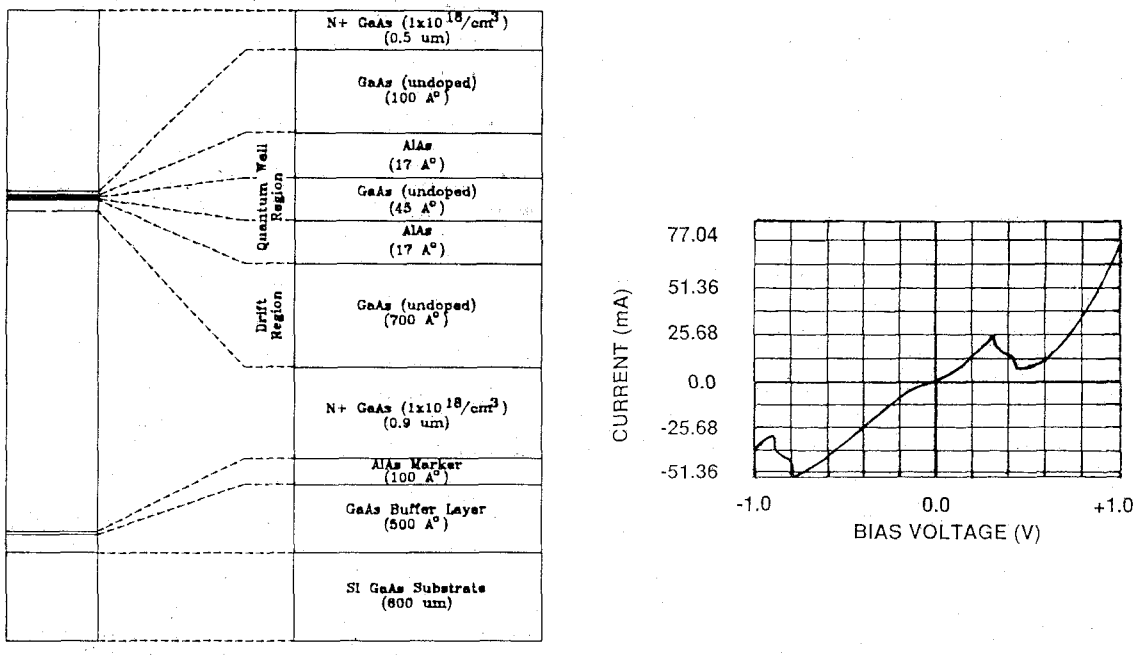

Fig. 1. (a) QWITT wafer structure. Wafers fabricated by Bell-Northern Research, Ottawa, Canada; processing by Communications Research Centre, Dept. of Communications, Ottawa, Canada; (b) Measured current–voltage characteristic for QWITT diode of 100 μm^2 cross-sectional area (quantum well consists of AlAs/GaAs/AlAs heterostructure of dimensions 20/45/20 Å, drift region length is 1.5 μm).

the electric field at N discrete points in the QWITT diode. The normal (canonical) form of the system of equations is defined as

$$\dot{\boldsymbol{x}}(t) = \boldsymbol{A}\boldsymbol{x}(t) + \boldsymbol{B}\boldsymbol{u}(t) \tag{1}$$

and

$$\boldsymbol{y}(t) = \boldsymbol{C}\boldsymbol{x}(t) + \boldsymbol{D}\boldsymbol{u}(t) \tag{2}$$

where

- $\boldsymbol{x}$ is a vector of state variables of dimension N;
- $\boldsymbol{u}$ is a vector of input variables of dimension M;
- $\boldsymbol{A}$ is the characteristic matrix of the system of dimension $N \times N$;
- $\boldsymbol{B}$ is a $N \times M$ matrix that relates the input variables to the system;
- $\boldsymbol{y}$ is the output vector of length J;
- $\boldsymbol{C}$ is a $J \times N$ matrix that relates $\boldsymbol{x}$ to $\boldsymbol{y}$;
- $\boldsymbol{D}$ is a $J \times M$ matrix that relates $\boldsymbol{u}$ to $\boldsymbol{y}$;

and $(\cdot)$ represents the time derivative.

The time-domain solution for the system is given by

$$\boldsymbol{x}(t) = e^{\boldsymbol{A}t}\boldsymbol{x}(0) + \int_0^t e^{\boldsymbol{A}(t-\tau)}\boldsymbol{B}\boldsymbol{u}(\tau)\, d\tau. \tag{3}$$

Here the state variable $\boldsymbol{x}(t)$ is completely determined by the initial conditions $\boldsymbol{x}(0)$ and the input $\boldsymbol{u}(\tau)$.

The frequency-domain response of the system is found by taking the Laplace transform of the normal form (eqs. (1) and (2)) with the result

$$\tilde{\boldsymbol{Y}}(s) = \boldsymbol{C}(s\boldsymbol{I} - \boldsymbol{A})^{-1}\boldsymbol{B}\tilde{\boldsymbol{U}}(s) + \boldsymbol{D}\tilde{\boldsymbol{U}}(s) \tag{4}$$

where $s = j\omega$ is the complex radian frequency and $\boldsymbol{I}$ is the identity matrix. Equation (4) is the principal result of this section, to be used in the derivation of the QWITT diode device model. The natural resonant frequencies of the system are given by the complex eigenvalues of the $\boldsymbol{A}$ matrix, where the real part gives the system damping factor and the imaginary part gives the resonant frequencies. This feature is extremely useful for studying oscillators and low-frequency stability problems.

III. Transient Carrier Transport

Transient transport effects in the drift region of the device must be included in order to construct an accurate device model [7]. Nonuniform carrier velocity results from the injection of electrons of high energy and, hence, high velocity into the drift region, with the carrier velocity subsequently decaying towards a steady-state saturated drift velocity, v_{sat}, at approximately 700 Å from the injection plane [7]. Also, according to Monte Carlo simulations conducted by Glisson *et al.* [14], the carrier diffusivity is a function of time. Our carrier transport analysis follows the technique of Botula *et al.* [7] and Song *et al.* [12] for carrier velocity. Since the diffusion component of the current is relatively small, we approximate the diffusivity with its constant steady-state value of $D_0 = 15\ cm^2/s$.

The carrier velocity v and position x as functions of time are given by [7]

$$v(t) = \Delta v e^{-t/\tau} + v_{sat} \tag{5}$$

and

$$x(t) = v_{sat}t + \tau\Delta v(1 - e^{-t/\tau}) \tag{6}$$

where v_{sat} is the saturated carrier velocity in the drift region, v_{peak} is the peak carrier velocity in the drift region, τ is the velocity time constant, which is taken as 8×10^{-14} s, and $\Delta v = v_{peak} - v_{sat}$.

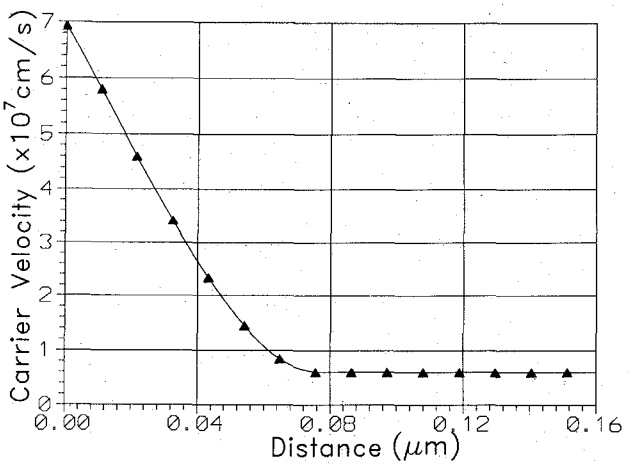

Fig. 2. Carrier drift velocity ▲ as a function of position in the drift region ($v_{peak} = 7\times10^7$ cm/s, $v_{sat} = 6\times10^6$ cm/s, $\tau = 8\times10^{-14}$ s). The origin is located at the injection plane defined by the quantum well region.

In order to implement the state-space model of the device, we have used (5) and (6) to determine the transient velocity as a function of position in the drift region of the device. Fig. 2 shows the relationship for the carrier drift velocity as a function of x for the case of $v_{sat} = 6\times10^6$ cm/s, $v_{peak} = 7\times10^7$ cm/s, and $\tau = 0.08$ ps. The graph represents a third-order curve fit to (5) and (6).

IV. The State-Space Model of the QWITT Diode

The state-space analysis approach is essentially a method of finding a solution to the one-dimensional equation

$$D(x)\frac{d^2E(x,t)}{dx^2} - v(x)\frac{dE(x,t)}{dx} + \frac{J_t}{\epsilon_d} = \frac{dE(x,t)}{dt} \quad (7)$$

which arises from the continuity equation

$$J_t = \epsilon_d\frac{dE(x,t)}{dt} - qn(x,t)v(x) + qD(x)\frac{dn(x,t)}{dx} \quad (8)$$

together with Poisson's equation:

$$n(x) = \frac{-\epsilon_d}{q}\frac{dE(x,t)}{dx} \quad (9)$$

where $v(x)$ is the electron velocity, $n(x)$ is the electron density, J_t is the total current density, $D(x)$ is the electron diffusivity, and ϵ_d is the dielectric constant in the drift region.

A variable cross-sectional diode area is accounted for in this analysis by modeling current flow in the drift region as laminar; i.e., the total current is assumed constant with respect to distance x and thus the current density is constant over any diode cross section that is perpendicular to the x direction. This approximation will be valid only for tapers that vary smoothly with distance through the drift region.

The model used in this paper for the QWITT is linear where we have used the large field velocity profile for the drift region. In our analysis, we inject a current from a constant current source, calculate the resulting voltage, and then compute the device impedance from the relation $Z = V/I$, where V is the complex phasor of the terminal voltage and I is the phasor of the injected current. This allows us to normalize the current density at any single position in the device.

In addition, the analysis rests on the assumption that the response of the quantum well structure to the applied electric field is instantaneous. That is, the quantum well analysis is quasi-static. This assumption is appropriate up to approximately 300 GHz [15].

State-space modeling proceeds by dividing the quantum well and drift regions of the QWITT device into N elements. Such a discretization, in effect, allows for the numerical solution of (7). Current continuity equations are then written at element boundaries, corresponding to the general state equation formulation described above. With reference to Fig. 3, the following terms are defined in the state-space model of the QWITT:

A_k = cross-sectional area of the kth slice (cm^2),
Δx = elemental width (cm),
V_k = volume of the kth element (cm^3),
n_k = electron density within the kth element (cm^{-3}),
Q_k = charge contained within the kth element (C),
E_k = electric field at the kth slice (V/cm),
v_k = average electron velocity at the kth slice (cm/s),
D_k = electron diffusivity at the kth slice (cm^2/s),
J_{ck} = conduction current density at the kth slice (A/cm^2),
J_{dk} = displacement current density at the kth slice (A/cm^2).

By way of further nomenclature, the kth element is bounded by slices of area A_{k-1} (i.e., the cross-sectional area of the right-hand boundary of the $(k-1)$th element) and A_k. Tapered diodes are accounted for by the inclusion of cross-sectional area in the formulation, and in this case, elements are truncated-pyramidal in shape.

The total current density flowing inside a semiconductor can be written as the sum of displacement, drift, and diffusion current density components. In formulating the state-space model we are interested in expressing the total current density, J_t, as the sum of these current components for each of the k elements, i.e.,

$$J_t = J_{\text{displacement},k} + J_{\text{drift},k} + J_{\text{diffusion},k}. \quad (10)$$

Displacement current arises within a semiconductor as a consequence of time-varying electric fields within the insulating material; i.e., particle currents are not responsible for current flow but it is the change in dielectric polarization which maintains current continuity across the semiconductor [16]. This dielectric displacement current density is expressed as $J_{\text{displacement}} = \partial D/\partial t$, where D is the dielectric displacement vector. For a linear dielectric,

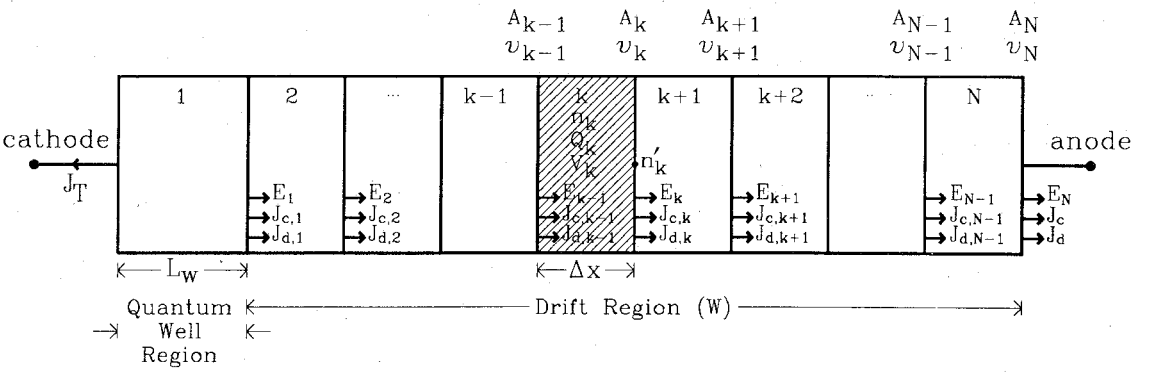

Fig. 3. State-space model representation for the QWITT. The RTD is divided into N elements with $N-1$ elements of width Δx describing the drift region. $J_{c,k}$ and $J_{d,k}$ are the conduction and displacement current densities, respectively, A_k is the cross-sectional area, v_k is the electron particle velocity, and E_k is the electric field at the right boundary of the kth element. V_k is the volume of the kth element, n_k is the electron density, and Q_k is the amount of charge contained within the kth element.

$D \equiv \epsilon_d E$, where ϵ_d is the dielectric constant and E is the electric field vector [16]. Therefore, the displacement current density at the kth slice (caused by the kth element) can be expressed as

$$J_{\text{displacement},k} = \epsilon_d \dot{E}_k. \tag{11}$$

It is to be noted that in Fig. 3 the first element in the state-space model describes the quantum well region, while the remaining $N-1$ elements describe the drift region of the device. For the first element, the diffusion contribution is neglected owing to the tunneling process in the quantum well region. Thus the total current density, J_t, is given by

$$J_t = \epsilon_d \dot{E}_1 + J_{\text{drift},1}. \tag{12}$$

The drift current density is simply determined by the injection conductance of the quantum well region, i.e., $J_{\text{drift},1} = \sigma_{\text{qw}} \cdot E_1$. Therefore, for the first element,

$$\dot{E}_1 = -\frac{\sigma_{\text{qw}}}{\epsilon_d} \cdot E_1 + \frac{1}{\epsilon_d} J_t. \tag{13}$$

On comparison with (1), it is apparent that (13) has the generalized state equation form where the electric field and total current density correspond to state variables x and u, respectively.

By definition, for low electric fields, the electron conduction current density is written as [17]

$$J_{\text{conduction}} = -q\mu_n nE + qD_n \nabla n \tag{14}$$

where μ_n is the electron mobility ($\text{cm}^2/\text{V}\cdot\text{s}$) and D_n is the diffusion constant (cm^2/s). For high electric fields, $\mu_n \cdot E$ is given by the saturated drift velocity [17], but since transient transport effects cannot be neglected [14], a more general expression for the conduction current density is

$$J_{\text{conduction}} = -qnv + qD\nabla n \tag{15}$$

where v is the electron particle velocity and D is the electron diffusivity.

The drift current density component is identified as the first term of (15), and the contribution for the kth element is written as

$$J_{\text{drift},k} = -qn'_k v_k \tag{16}$$

where q is the unit of electron charge, v_k is the average electron particle velocity, and n'_k is the density of electrons at the kth slice, approximated as the average of electron densities for the kth and $(k+1)$th elements.

Gauss's law requires that, over a closed surface, the surface integral of the normal component of the electric field be equal to the sum of charges inside the enclosed volume divided by the dielectric constant. Since the kth slice is located at the center of the kth and $(k+1)$th elements, we consider both elements in applying Gauss's law. Approximating the electron density for the complete volume as n'_k, the total charge is given by $Q_k + Q_{k+1} = -qn'_k(V_k + V_{k+1})$. With reference to Fig. 3, it is apparent that the input and output fluxes for the volume defined by the kth and $(k+1)$th elements are $\epsilon_d \cdot A_{k-1} \cdot E_{k-1}$ and $\epsilon_d \cdot A_{k+1} \cdot E_{k+1}$, respectively. Therefore, Gauss's law is expressed as $-qn'_k(V_k + V_{k+1}) = \epsilon_d[A_{k+1} \cdot E_{k+1} - A_{k-1} \cdot E_{k-1}]$. Solving for the charge density and substituting into (16) then gives the drift current density for the kth element:

$$J_{\text{drift},k} = \frac{\epsilon_d v_k}{V_k + V_{k+1}}[A_{k+1} \cdot E_{k+1} - A_{k-1} \cdot E_{k-1}]. \tag{17}$$

For the kth element, the diffusion current density component of (15) is written as

$$J_{\text{diffusion},k} = qD_k \frac{\partial n_k}{\partial x} \approx qD_k \left\{ \frac{n_{k+1} - n_k}{\Delta x} \right\}$$

where D_k is defined as the electron particle diffusivity at the kth slice and the derivative is approximated by the difference in electron density between the $(k+1)$th and kth elements divided by the elemental width, Δx. As above, Gauss's law is applied in determining the charge densities for the kth and $(k+1)$th elements, and the diffusion current density becomes

$$J_{\text{diffusion},k} = \frac{\epsilon_d D_k}{\Delta x V_k V_{k+1}}[\{-A_{k-1}V_{k+1}\}E_{k-1} + A_k\{V_k + V_{k+1}\}E_k - \{A_{k+1}V_k\}E_{k+1}]. \tag{18}$$

Adding the contributions from displacement, drift, and diffusion components (eqs. (11), (17), and (18), respectively) yields the total electron current density, J_t. Rearranging in terms of $\dot{E}_k$ and collecting electric field terms defines the system of state equations for elements 2 to $N-1$:

$$\dot{E}_k = \frac{1}{\epsilon_d} J_t + A_{k-1}\left[\frac{v_k}{V_k + V_{k+1}} + \frac{D_k}{\Delta x \cdot V_k}\right] \cdot E_{k-1} - \left[\frac{D_k \cdot A_k\{V_k + V_{k+1}\}}{\Delta x \cdot V_k \cdot V_{k+1}}\right] \cdot E_k + A_{k+1}\left[\frac{D_k}{\Delta x \cdot V_{k+1}} - \frac{v_k}{V_k + V_{k+1}}\right] \cdot E_{k+1}. \quad (19)$$

For the drift and diffusion current density components of the Nth element, the charge density at the right-hand boundary of the drift region is approximated through a parabolic interpolation in the drift region. This is a second-degree extrapolation of the adjacent charge density values and is useful for minimizing slope discontinuity at the boundary, particularly for the diffusion term. Given the equation for a parabola, $f[k] = ak^2 + b$, it can be shown that $f[0] = 4/3 f[1] - 1/3 f[2]$. Using this result, the charge density at the right-hand boundary of the Nth element, n'_N, is written as

$$n'_N = \frac{4}{3} n_N - \frac{1}{3} n'_{N-1}.$$

The derivative involved in the diffusion current density contribution, however, requires the charge density gradient across the boundary. Considering an $(N+1)$th element, parabolic interpolation is again used, and based on charge density values in the drift region, the charge density at the center of this element is approximated as

$$n_{N+1} = \frac{4}{3} n'_N - \frac{1}{3} n_N.$$

Thus, for the Nth element, the expression for the total current density, J_t, becomes

$$J_t = \epsilon_d \dot{E}_N - q v_N n'_N - \frac{n_{N+1} - n_N}{\Delta x}. \quad (20)$$

Applying Gauss's law and rearranging in terms of $\dot{E}_N$ gives

$$\dot{E}_N = \frac{1}{\epsilon_d} J_t - \frac{A_{N-2}}{(V_{N-1} + V_N)} \cdot \left[\frac{v_N}{3} + \frac{4D_N}{9\Delta x}\right] \cdot E_{N-2} + \frac{4A_{N-1}}{V_N} \cdot \left[\frac{v_N}{3} + \frac{D_N}{9\Delta x}\right] \cdot E_{N-1} + A_N \cdot \left[-\frac{4v_N}{3V_N} + \frac{v_N}{3(V_{N-1} + V_N)} - \frac{4D_N}{9\Delta x V_N} + \frac{4D_N}{9\Delta x (V_{N-1} + V_N)}\right] \cdot E_N. \quad (21)$$

Equations (13), (19), and (21) form a set of equations with the generalized matrix form

$$\dot{\boldsymbol{E}} = \boldsymbol{A}\boldsymbol{E} + \frac{1}{\epsilon_d} \boldsymbol{J}_t \quad (22)$$

where the $\boldsymbol{A}$ matrix is written as

$$\boldsymbol{A} = \begin{array}{c} \begin{matrix} 1 & 2 & 3 & \cdots & k-1 & k & k+1 & \cdots & N-2 & N-1 & N \end{matrix} \\ \begin{bmatrix} -\frac{\sigma_{qw}}{\epsilon_d} & 0 & 0 & \cdots & 0 & 0 & 0 & \cdots & 0 & 0 & 0 \\ X_{21} & Y_{22} & Z_{23} & \cdots & 0 & 0 & 0 & \cdots & 0 & 0 & 0 \\ \vdots & \vdots & \vdots & & \vdots & \vdots & \vdots & & \vdots & \vdots & \vdots \\ 0 & 0 & 0 & \cdots & X_{k,k-1} & Y_{k,k} & Z_{k,k+1} & \cdots & 0 & 0 & 0 \\ \vdots & \vdots & \vdots & & \vdots & \vdots & \vdots & & \vdots & \vdots & \vdots \\ 0 & 0 & 0 & \cdots & 0 & 0 & 0 & \cdots & X_{N,N-2} & Y_{N,N-1} & Z_{N,N} \end{bmatrix} \end{array}$$

and

$$X_{k,k-1} = A_{k-1} \cdot \left[\frac{v_k}{V_k + V_{k+1}} + \frac{D_k}{\Delta x \cdot V_k}\right]$$

$$Y_{k,k} = -\frac{D_k \cdot A_k\{V_k + V_{k+1}\}}{\Delta x \cdot V_k \cdot V_{k+1}}$$

$$Z_{k,k+1} = A_{k+1} \cdot \left[\frac{D_k}{\Delta x \cdot V_{k+1}} - \frac{v_k}{V_k + V_{k+1}}\right]$$

where $X_{N,N-2}$, $Y_{N,N-1}$, and $Z_{N,N}$ are defined as the electric field coefficients in (21).

Equation (22) has the general state equation form of (1), expressing the time-domain behavior of electrons within the RTD in terms of current and electric field. Applying Laplace transformation, and assuming the total current density to be normalized to unity, the frequency-domain response of the RTD becomes

$$\tilde{\boldsymbol{E}}(s) = (s\boldsymbol{I}_{N\times N} - \boldsymbol{A})^{-1} \frac{1}{\epsilon_d} \boldsymbol{I}_{N\times 1}. \quad (23)$$

where $\boldsymbol{I}_{N\times N}$ is the square identity matrix and $\boldsymbol{I}_{N\times 1}$ is a unit column vector. Given the electric field, the total voltage across the device, relative to the cathode, can be

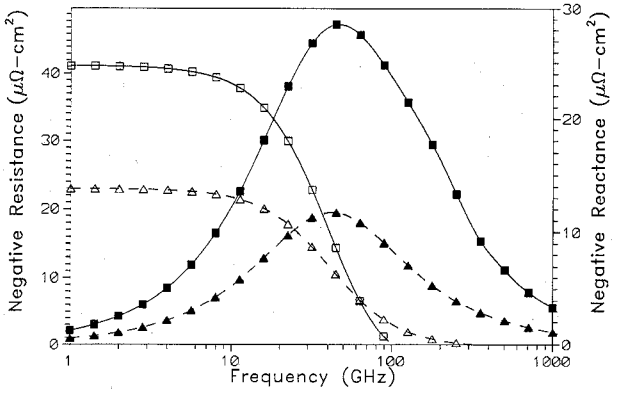

Fig. 4. Device impedance (nontapered QWITT, $L_w = 0.01$ μm, $\sigma = -300$ mS·cm) versus frequency for varying drift region length as calculated using the state-space model (uniform velocity profile with $v(x) = v_{sat} = 6\times10^6$ cm/s, diffusion effects not included): ——— drift region = 0.23 μm; --- drift region length = 0.07 μm. Symbols correspond to results computed using the analytic solution obtained by Kesan *et al.* [8]: □, ■ resistive and reactive components, respectively, $W = 0.23$ μm; △, ▲ resistive and reactive components, respectively, $W = 0.07$ μm.

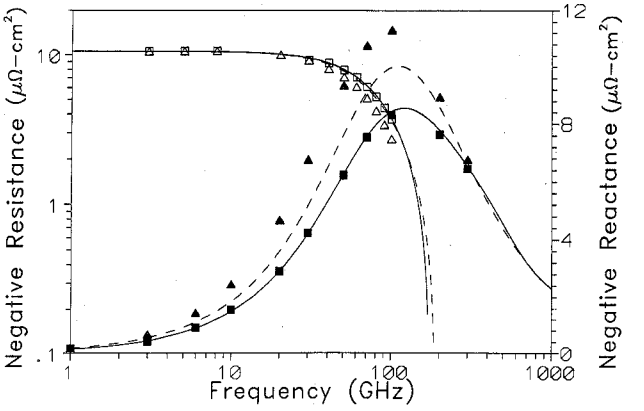

Fig. 5. Device impedance (nontapered QWITT, $L_w = 75$ Å, $W = 0.16$ μm) versus frequency as calculated using (a) ——— state-space model (nonuniform velocity: $v_{peak} = 7\times10^7$ cm/s, $v_{sat} = 6\times10^6$ cm/s, $\tau = 8\times10^{-14}$ s, diffusion effects not included, $\sigma = -771.3$ mS·cm); (b) --- state-space model (nonuniform velocity, including diffusion effects, $\sigma = -728.5$ mS·cm). Symbols correspond to results reported by Botula and Wang [7]: □, ■ resistive and reactive components, respectively (nonuniform velocity, diffusion effects not included, $\sigma = -781$ mS·cm); △, ▲ resistive and reactive components, respectively (nonuniform velocity, including diffusion effects, $\sigma = -658$ mS·cm).

written as

$$\tilde{V}_t(s) = \{L_w + \Delta x/2\}\tilde{E}_1(s) + \sum_{k=1}^{N} \tilde{E}_k(s)\Delta x + \frac{\Delta x}{2}E_N(s)$$
$$= \tilde{J}_t(s)\tilde{Z}(s) \qquad (24)$$

and since unity current density has been assumed, the normalized device impedance $\tilde{Z}(s)$ in $\Omega\cdot\text{cm}^2$ is directly obtained.

V. Comparison with Previous Results

To confirm the validity of the state-space approach, we have compared our results with previously reported analytic solutions. Specifically, we have compared the state-space results with the models of Kesan *et al.* [8] for ideal devices and with the models of Botula *et al.* [7] that include nonsaturated drift velocity and diffusion effects.

The comparison of the state-space formulation with the analytic solution of Kesan *et al.* is presented in Fig. 4 for diodes with varying drift region length ($W = 0.23$ and 0.07 μm). In all cases, the drift velocity is assumed to be saturated at a value of 6×10^6 cm/s, with the injection conductance taken to be -300 mS·cm. At this point, diffusion effects are not taken into consideration. For state-space analysis, we have found that it is necessary to subdivide the drift region into elements that are no greater than one tenth of a wavelength in width at the maximum frequency of interest. In this case, the wavelength is 0.06 μm at a frequency of 1000 GHz, which means that the drift region must be subdivided into at least 38 elements. For our analysis, we have used 75 elements in all cases. The small-signal negative impedance of the diodes as shown in Fig. 4 agrees very well with the analytic solution of Kesan *et al.* [8] for all cases studied and for frequencies up to 1000 GHz.

We have also compared the state-space method with the results of Botula *et al.* in modeling transient transport effects in the drift region. The two cases studied are nonuniform carrier velocity not including diffusion and nonuniform velocity including the effect of diffusion. As described above in Section III, we use the same velocity profile as Botula *et al.* (shown previously in Fig. 2) and assume a constant diffusivity of $D_0 = 15$ cm^2/s. For this analysis $N = 500$ and, in all cases, the diodes are assumed to be of constant cross-sectional area and a series parasitic resistance of 2 $\mu\Omega\cdot\text{cm}^2$ is included, as in [7]. All injection conductance values have been adjusted such that the device impedance is normalized to -10.6 $\mu\Omega\cdot\text{cm}^2$ at low frequency, allowing for a direct comparison with the modeling by Botula *et al.* The results of this study are given in Fig. 5, where the real and imaginary parts of the small-signal impedance are given for the two cases.

In the first case, the device impedance predicted using the state-space model agrees very well with the solution obtained by Botula *et al.* Differences are apparent, however, when the effects of diffusion are included. In this case, the state-space model predicts a slightly higher cutoff frequency for the resistive component than that predicted by the diffusionless model, whereas Botula *et al.* predict a lower frequency cutoff. On further comparison, for the state-space model the inclusion of diffusion results in a lower reactive component at the resonant frequency; since there is closer correspondence between resistive components for the two cases, this implies that diffusion has a smaller effect on the device impedance than previously reported. Furthermore, given the differences in injection conductance required to normalize the low-frequency negative resistance to 10.6 $\mu\Omega\cdot\text{cm}^2$ for cases including and excluding diffusion (42.8 mS·cm for the state-space model versus 123 mS·cm reported by Botula *et al.*), this also implies that the state-space model

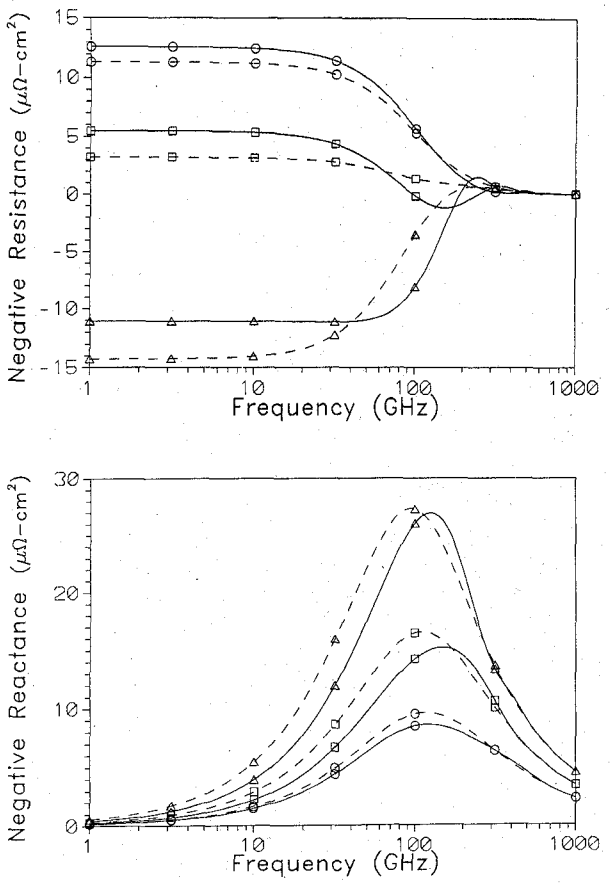

Fig. 6. Device impedance (nontapered QWITT, $L_w = 75$ Å, $W = 0.16$, 0.24, 0.32 μm) versus frequency as calculated using the state-space model including and excluding diffusion (injection conductance $\sigma = -771.3$ mS·cm, identical for both formulations, $v_{peak} = 7\times10^7$ cm/s, $v_{sat} = 6\times10^6$ cm/s, $\tau = 8\times10^{-14}$ s): ——— state-space model excluding diffusion effects; ---- state-space model including diffusion effects; ○ $W = 0.16$ μm; □ $W = 0.24$ μm; △ $W = 0.32$ μm.

predicts that diffusion affects the device impedance less than the modeling proposed by Botula *et al.*

VI. New Results

In this section, we report new results for the performance and modeling of active and passive RTD's. These results include the effect of diffusion on the impedance of RTD's of various lengths, the performance of long diodes with a positive injection conductance, and a demonstration of the traveling wave nature of current, charge, and electric field in the drift region.

Initially, we have studied the quantitative effects of diffusion on the impedance of active diodes of negative injection conductance for various diode lengths. For this study, we have selected a typical RTD with a quantum well length of 75 Å and an injection conductance of -771.3 mS·cm. The impact of diffusion on the real part of the RTD impedance is shown in Fig. 6(a), where the RTD impedance is plotted versus frequency for drift region lengths of 0.16, 0.24, and 0.32 μm. For each diode configuration, we have plotted the impedance using the complete model, velocity profile and diffusion included,

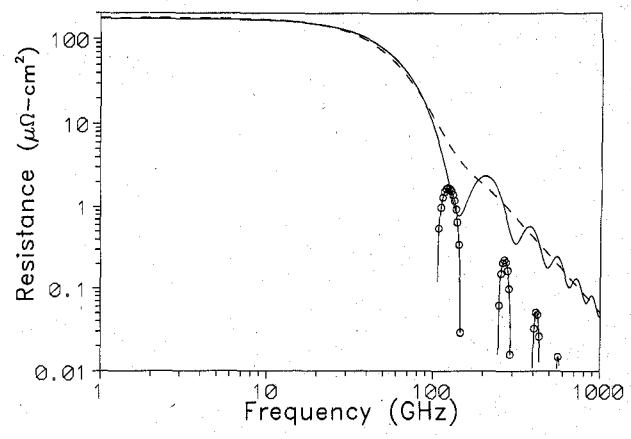

Fig. 7. Resistance versus frequency (nontapered QWITT, $L_w = 0.01$ μm, $W = 0.4$ μm, $\sigma = +500$ mS·cm): ○ negative resistance as calculated using analytic solution obtained by Kesan *et al.* [8]; ——— positive resistance as calculated using state-space model with non-constant-velocity profile ($v_{peak} = 7\times10^7$ cm/s, $v_{sat} = 6\times10^6$ cm/s, $\tau = 8\times10^{-14}$ s), neglecting diffusion; ---- positive resistance as calculated using state-space model with non-constant-velocity profile, including diffusion.

and the model where the diffusion term of the current is neglected. It is seen in Fig. 6(a) that in all cases the effect of diffusion adds a positive component to the RTD resistance and that the effect is more pronounced for long diodes. For short diodes ($W = 0.16$ μm), the diffusion current reduces the negative resistance for low frequencies by approximately 12%. The reactive component of the impedance is shown in Fig. 6(b). Here it is noted that the agreement between models with respect to the predicted resonant frequency improves as the drift region length decreases.

We now consider the performance of long diodes that have a positive quantum-well injection conductance. Previous results [8] indicate that even with a positive conductance, the RTD will still exhibit a negative device impedance for certain values of the drift region length and quantum well admittance. Basically, the drift region length must be near a multiple of one wavelength at the operating frequency if it is to produce a negative impedance. In agreement with the results reported in [12], our results confirm that these devices do not exhibit negative impedance at any frequency because of the combined effects of diffusion current and a nonconstant velocity profile in the drift region. This is demonstrated in Fig. 7, where the RTD resistance, positive or negative, is plotted as a function of frequency for a diode with an injection conductance of $+500$ mS·cm and a drift region length of 0.4 μm. The analytic solution of Kesan *et al.* [8] shows that this diode exhibits a negative resistance in the region of 120 GHz. The case where the velocity profile and diffusivity are included shows that the resistance is positive for all frequencies, approaching zero at high frequency and 140 $\mu\Omega\cdot$cm^2 at low frequency, as expected. Similarly, for the case where diffusion is ignored but the velocity profile is included, the diode resistance is always positive with asymptotic behavior, as before, but now shows a fairly strong oscillation with frequency.

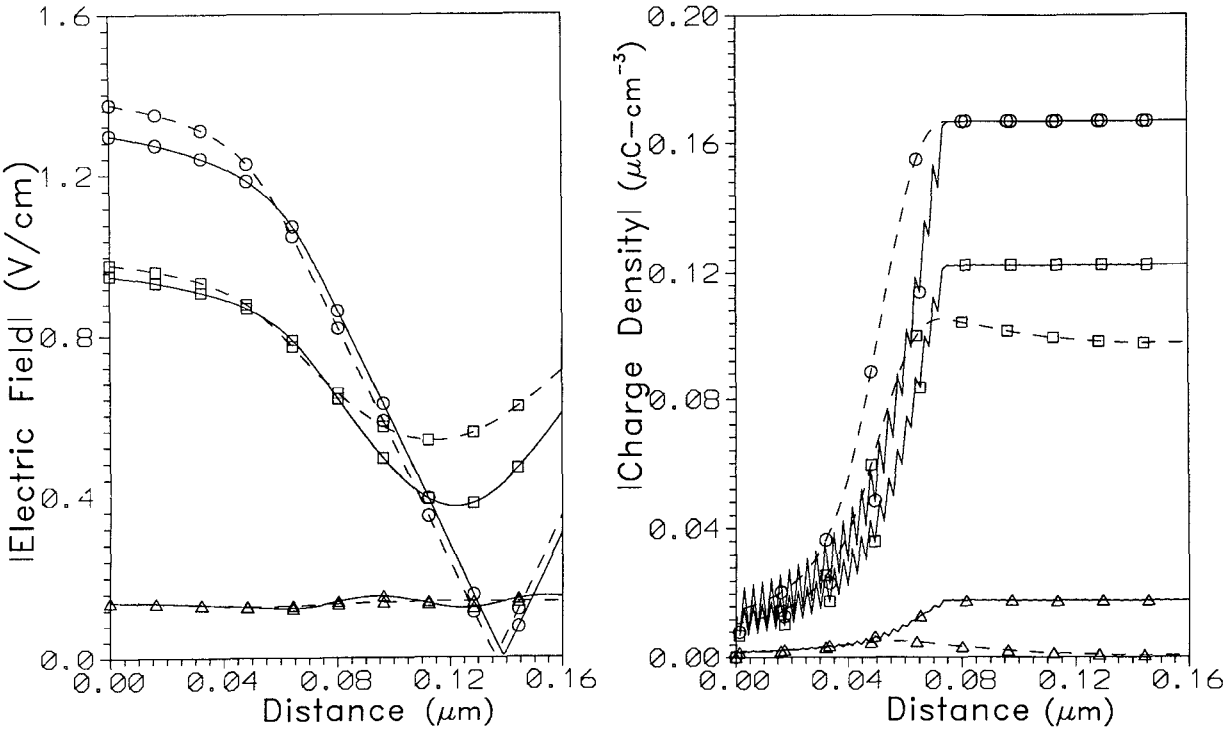

Fig. 8. Small-signal phasor magnitudes of (a) electric field and (b) charge density versus position in the drift region (nontapered QWITT, $L_w = 75$ Å, $W = 0.16$ μm) for three different frequencies: ○ 1 GHz (below resonance); □ 100 GHz (at resonance); △ 1000 GHz (above resonance). The origin is located at the injection plane, defined by the quantum well region. ——— Calculated using state-space model, $\sigma = -771.3$ mS·cm, non-constant-velocity profile ($v_{peak} = 7\times10^7$ cm/s, $v_{sat} = 6\times10^6$ cm/s, $\tau = 8\times10^{-14}$ s), neglecting diffusion; ---- calculated using state-space model, $\sigma = -728.5$ mS·cm, with non-constant-velocity profile, including diffusion.

As given by (23), the electric field at each of the defined elements, hence as a function of position in the QWITT, directly results from the state-space modeling approach. Given the elemental electric field, the charge density, as well as the current density, components are readily obtained. Fig. 8 shows the magnitudes of the elemental electric field and charge density for nonuniform velocity formulations including and excluding diffusion for three different frequencies: 1 GHz (below resonance), 100 GHz (at resonance), and 1000 GHz (above resonance). Physical QWITT parameters are as previously studied, with the corresponding impedance versus frequency shown in Fig. 5.

Two features are immediately apparent in considering Fig. 8. First, the electric field and charge density appear to be complementary as a function of position. For example, for the 1 GHz case, the electric field decays across the RTD while the charge density increases to an equilibrium value. Second, both the electric field and the charge density decrease in magnitude with frequency while differences in the charge density for formulations including and excluding diffusion increase with frequency. It is to be noted that the wavelength of oscillations apparent in the electric field for the 1000 GHz, diffusionless case corresponds to 0.06 μm, as expected, demonstrating the traveling wave nature of carrier transport in the drift region.

Fig. 9 shows the magnitudes of the current density components for the same parameters as in Fig. 8. In general, the displacement current density component dominates at higher frequencies, while the drift current component dominates at lower frequencies and the diffusion current appears to offer a relatively small contribution. An important feature to note is the peak in drift and diffusion current density components (for the formulation including diffusion) occurring at 0.05 μm. However, these current density components are in phase opposition so that the conduction current, given by the sum of the drift and diffusion components, roughly corresponds to the drift component for the diffusionless formulation. Again, oscillations in the displacement current density for the 1000 GHz, diffusionless case have a wavelength of 0.06 μm.

VII. Conclusion

We have presented a state-space model of the QWITT diode and confirmed its accuracy through comparison with previous analytical solutions obtained by Kesan *et al.* and Botula *et al.* The comparison showed that the state-space method agrees with previous models in most cases. In agreement with results obtained by Song *et al.*, one significant difference is that for diodes with a positive injection conductance and a long drift region, our models

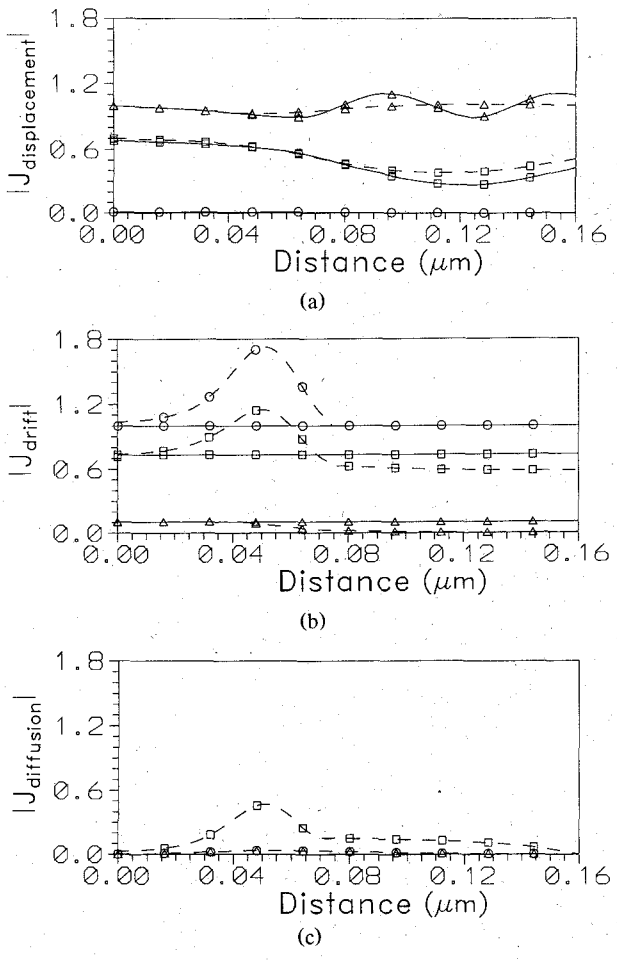

Fig. 9. Small-signal phasor magnitudes of (a) displacement, (b) drift, and (c) diffusion current density components versus position in the drift region (nontapered QWITT, $L_w = 75$ Å, $W = 0.16$ μm) for three different frequencies: ○ 1 GHz (below resonance); □ 100 GHz (at resonance); △ 1000 GHz (above resonance). The origin is located at the injection plane defined by the quantum-well region. ——— Calculated using state-space model, $\sigma = -771.3$ mS·cm, non-constant-velocity profile ($v_{peak} = 7\times10^7$ cm/s, $v_{sat} = 6\times10^6$ cm/s, $\tau = 8\times10^{-14}$ s), neglecting diffusion; ---- calculated using state-space model, $\sigma = -728.5$ mS·cm, non-constant-velocity profile, including diffusion.

do not predict a negative real part of the device input impedance, as predicted by the model of Kesan *et al.* The input impedance always has a positive real part because of the damped traveling wave nature of the displacement current in the drift region. This only becomes evident when carrier diffusivity and velocity profiles are considered. A second difference noted was that the state-space model indicates that carrier diffusion has a smaller effect on the device impedance than predicted by Botula *et al.*

The state-space method is readily suited to the analysis of diodes and the circuits in which they are embedded. It is also particularly useful for the study of millimeter-wave oscillators since the eigenvalues of the complete system are contained in the system matrix. It is expected that this technique can be extended to many circuit and device applications. A prime candidate for the application of this technique is the optical p-i-n photo detector diode, which is useful in high-speed applications. Generation and recombination processes must be included in the analysis of the p-i-n diode, an extension that is now being considered.

We have found that the state-space modeling approach to transit-time-limited devices provides a great deal of insight into the physical process within the diode. For example, the traveling wave natures of all currents, fields, and charge densities are a natural outcome of the analysis. This method of analysis is directly useful for time-domain analysis and time-domain nonlinear simulation since the state equations can be implemented directly in SPICE computer programs.

Acknowledgment

The authors are indebted to Dr. O. Berolo of the Communications Research Centre, Ottawa, Canada, for encouragement given us throughout the QWITT Diode research program, and to the reviewers for their indepth critique.

References

[1] R. Tsu and L. Esaki, "Tunneling in a finite superlattice," *Appl. Phys. Lett.*, vol. 22, no. 11, pp. 562–564, June 1973.
[2] P. D. Bauman, D. R. Conn, K. L. Wu, and J. Litva, "Integrated antenna design using resonant tunneling diodes," in *Proc. ANTEM Symp. Antenna Technol. and Appl. Electromagn.* (Winnipeg, Canada), Aug. 1990.
[3] P. M. Smith, D. R. Conn, and J. Xu, "The limits of resonant tunneling diode subharmonic mixer performance," *J. Appl. Phys.*, vol. 66, no. 3, pp. 1454–1458, Aug. 1989.
[4] V. P. Kesan, A. Mortazawi, D. P. Neikirk, and T. Itoh, "Microwave and millimetre-wave QWITT diode oscillator," in *IEEE-MTT-S Int. Microwave Symp. Dig.*, June 1989, pp. 487–490.
[5] E. R. Brown, T. C. L. G. Sollner, C. D. Parker, W. D. Goodhue, and C. L. Chen, "Oscillations up to 420 GHz in GaAs/AlAs resonant tunneling diodes," *Appl. Phys. Lett.*, vol. 55, no. 7, pp. 1777–1779, Oct. 1989.
[6] J. M. Owens, D. J. Halchin, K. L. Lear, W. S. Lee, and J. S. Harris, Jr., "Microwave characteristics of MBE grown resonant tunneling devices," in *IEEE MTT-S Int. Microwave Symp. Dig.*, June 1989, pp. 471–474.
[7] A. Botula and K. L. Wang, "Improved small-signal analysis of the quantum-well injection transit time diode," *IEEE Trans. Electron Devices*, vol. 37, pp. 58–65, Jan. 1990.
[8] V. P. Kesan, D. P. Neikirk, B. J. Streetman, P. A. Blakey, and T. D. Linton, Jr., "The influence of transit-time effects on the optimum design and maximum oscillation frequency of quantum well oscillators," *IEEE Trans. Electron Devices*, vol. 35, pp. 405–413, Apr. 1988.
[9] W. T. Read, "A proposed high-frequency negative resistance diode," *Bell Syst. Tech. J.*, vol. 37, pp. 401–446, 1958.
[10] M. Gilden and M. F. Hines, "Electronic tuning effects in the Read microwave avalanche diode," *IEEE Trans. Electron Devices*, vol. ED-13, pp. 169–175, 1966.
[11] C. Kidner, I. Mehdi, J. R. East, and G. I. Haddad, "Power and stability limitations of resonant tunneling diodes," *IEEE Trans. Microwave Theory Tech.*, vol. 38, pp. 864–872, July 1990.
[12] I. Song and D. Pan, "Analysis and simulation of the quantum well injection transit time diode," *IEEE Trans. Electron Devices*, vol. 35, pp. 2315–2322, Dec. 1988.
[13] L. A. Zadeh and C. A. Desoer, *Linear System Theory*. Toronto: McGraw-Hill, 1963.
[14] T. H. Glisson, T. K. Williams, J. R. Hauser, and M. A. Littlejohn, "Transient response of electron transport in GaAs using Monte Carlo method," in *VLSI Electronics: Microstructure Science*, vol. 4, N. G. Einspruch, Ed. New York: Academic Press, 1982, pp. 99–145.
[15] D. S. Pan and C. C. Meng, "On the mechanism and frequency limit of double-barrier quantum-well structures," *J. Appl. Phys.*, vol. 61, no. 5, pp. 2082–2084, Mar. 1987.

[16] R. F. Pierret, *Advanced Semiconductor Fundamentals Modular Series on Solid State Devices*, vol. VI. Reading, MA: Addison-Wesley, 1989.
[17] S. M. Sze, *Physics of Semiconductor Devices*. New York: Wiley, 1981.

David R. Conn (S'68—M'88) received the B.Sc., M.Sc., and Ph.D. degrees in electrical engineering from Queen's University, Kingston, Ontario, Canada, in 1959, 1961, and 1970 respectively.

From 1970 to 1972, he was a guest scientist at the Institute for Microwaves, Stockholm, Sweden, where he conducted basic research on the circuit performance of Gunn and IMPATT millimeter-wave diodes. In 1972, he was appointed to the position of Associate Professor in the Department of Electronics and Materials at Carleton University, Ottawa, Canada. His research interests included the nonlinear modeling of microwave devices and circuits and CAD applications of microwave systems. From 1976 to 1987, he held the positions of research scientist and manager in the microwave radio division of Bell-Northern Research, Ottawa, Canada, where he developed microwave active components for digital radio systems and explored the signal processing capabilities of GaAs devices for industrial applications. He is presently Professor of Electrical and Computer Engineering at McMaster University, where he holds the NSERC/BNR Chair in Microwaves and is an associate member of the Engineering Physics Department. Dr. Conn is a member of the Communications Research Laboratory of McMaster University, the Telecommunications Research Institute of Ontario, and the Centre for Electrophonic Materials and Devices at McMaster University. His current research is in the area of very high speed optoelectronic devices and packaging for digital communication systems. This research includes the modeling of heterostructure devices, MSM photo detectors, and electro-optic sampling components.

Paul D. Bauman received the B.Sc. degree in physics from McMaster University, Hamilton, Canada, in 1983, followed by the M.Sc. degree in physics from the University of Waterloo, Waterloo, Canada, in 1985. While at Waterloo, his thesis research focused on the application of cepstral techniques to transducer measurement with other areas of interest including digital signal processing, sound recording techniques, and digital audio. In 1986 he joined the Communications Research Laboratory at McMaster University as a Research Engineer and he has recently completed the M.Eng. degree in electrical engineering based on the work described in this paper. Other areas of research at the Communications Research Laboratory have included MMIC design and testing, meteorological effects on low-angle tracking, sampled-aperture radar systems, sea swell and ocean multipath modeling, and high-resolution spectral estimation techniques.

He has remained actively involved in the professional audio field since 1983, serving as secretary for the Toronto Chapter of the Audio Engineering Society from 1986 to 1989, and as secretary for the AES International Conference on Digital Audio in 1989. He has also served as a technical writer for the magazines *Sound & Vision* and *Broadcast Technology* and has been an independent recording engineer/producer and a semiprofessional musician. He has recently accepted a one-year position as Guest Researcher in the Department of Applied Acoustics at Chalmers University of Technology, Gothenburg, Sweden, to study sound intensity in structures and structure-borne sound propagation. At the same time, he will maintain an affiliation with the Adamson Acoustic Design Corporation, serving as Audio Engineer in the development of DSP-based adaptive control electronics for advanced concert systems.

Mr. Bauman is a member of the Audio Engineering Society and a life member of the Communications Research Laboratory.